NASA Technical Memorandum 106609

A Fully Associative, Non-Linear Kinematic, Unified Viscoplastic Model for Titanium Based Matrices

S. M. Arnold
National Aeronautics and Space Administration
Lewis Research Center
Cleveland, Ohio

A. F. Saleeb
University of Akron
Akron, Ohio

and

M. G. Castelli
NYMA, Inc.
Engineering Services Division
Brook Park, Ohio

Prepared for the
Symposium on Life Prediction Methodology for Titanium Matrix Composites
sponsored by the American Society for Testing and Materials
Hilton Head, South Carolina, March 22–24, 1994

National Aeronautics and
Space Administration

Trade names or manufacturers' names are used in this report for identification only. This usage does not constitute an official endorsement, either expressed or implied, by the National Aeronautics and Space Administration.

A Fully Associative, Non-Linear Kinematic, Unified Viscoplastic Model for Titanium Based Matrices

S. M. Arnold
National Aeronautics and Space Administration
Lewis Research Center
Cleveland, Ohio 44135

A. F. Saleeb
University of Akron
Department of Civil Engineering
Akron, Ohio 44325

M. G. Castelli
NYMA, Inc.
Engineering Services Division
Brook Park, Ohio 44142

Abstract

Specific forms for both the Gibb's and complementary dissipation potentials are chosen such that a complete (i.e., fully associative) potential based multiaxial unified viscoplastic model is obtained. This model possess one tensorial internal state variable, that is associated with dislocation substructure, with an evolutionary law that has nonlinear kinematic hardening and both thermal and strain induced recovery mechanisms. A unique aspect of the present model is the inclusion of non-linear hardening through the use of a compliance operator, derived from the Gibb's potential, in the evolution law for the back stress. This non-linear tensorial operator is significant in that it allows both the flow and evolutionary laws to be fully associative (and therefore easily integrated) and greatly influences the multiaxial response under non-proportional loading paths. In addition to this nonlinear compliance operator, a new consistent, potential preserving, internal strain unloading criterion has been introduced to prevent abnormalities in the predicted stress-strain curves, which are present with nonlinear hardening formulations, during unloading and reversed loading of the external variables. Specification of an experimental program for the complete determination of the material functions and parameters for characterizing a metallic matrix, e.g., TIMETAL 21S, is given. The experiments utilized are tensile, creep, and step creep tests. Finally, a comparison of this model and a commonly used Bodner-Partom model is made on the basis of predictive accuracy and numerical efficiency.

Keywords: viscoplasticity, nonlinear hardening, isothermal, deformation, multiaxial, correlations, predictions

1 Nomenclature

Invariants

Ω	complementary dissipation potential
Φ	Gibb's complementary potential
F	Bingham-Prager threshold function
G, Ψ	normalized second invariant functions
J_2	second invariant of effective deviatoric stress tensor
I_2	second invariant of internal deviatoric stress tensor
H_1	invariant material functions

Stresses

σ_{ij}	Cauchy stress tensor
S_{ij}	deviatoric stress tensor
Σ_{ij}	effective deviatoric stress tensor
α_γ	internal state variables (stress-like)
α_{ij}	internal (or back) stress tensor
a_{ij}	deviatoric internal stress tensor
κ, κ_o	drag stress and initial drag stress
Y	yield stress

Strains

$e_{ij}, \epsilon^I_{ij}, \epsilon^R_{ij}, \epsilon^T_{ij}$	total, inelastic, reversable, and thermal strain tensors, respectively
$\mathcal{A}_\xi$	conjugate internal state variables (displacement-like)
$\mathcal{A}_{ij}$	internal strain tensor

Material Parameters

C_{ijkl}, E_{ijkl}	elastic compliance and stiffness tensor, respectively
B_0, B_1, R_α	hardening and thermal recovery material parameters
μ, κ	material parameters
β	denotes the extent of strain induced recovery
n, p, q	material exponents
$g(G), f(F)$	material functions
$\bar{E}(\sigma_{ij}), \bar{H}(\alpha_\gamma), Z(T)$	material functions
$\eta, \hat{E}, \hat{G}$	coefficient of thermal expansion, Young's modulus, shear modulus

Miscellaneous

T_{ref}	reference temperature
$sgn(\ )$	sign function: takes on 1 or -1 depending upon the sign of argument
Q_{ijkl}, L_{ijkl}	internal compliance and internal stiffness operators, respectively
δ_{ij}	Kronecker delta function
$\langle\ \rangle$	Macauley bracket
Hv[ ]	Heaviside unit function
$(\dot{\ })$	time derivative (or rate) notation
$\dot{\mathcal{S}}$	instantaneous state trajectory
$\dot{\mathcal{G}}, \dot{\mathcal{D}}$	components of the state trajectory, $\dot{\mathcal{S}}$.

2 Introduction

A number of Titanium Matrix Composite (TMC) systems are currently being researched and evaluated for high temperature air frame and propulsion system applications. As a result, numerous computational methodologies for predicting both deformation and life are under development. An integral part of these methodologies is an accurate and computationally efficient constitutive model for the metallic matrix constituent. Furthermore, because of the proposed elevated operation temperatures for which these systems are designed, the required constitutive models must account for both time-dependent and time-independent deformations. To accomplish this we will employ a recently developed complete potential based framework[1] utilizing internal state variables which was put forth for the derivation of reversible and irreversible constitutive equations. This framework, and consequently the resulting constitutive model, is termed complete because the existence of the total (integrated) form of the Gibbs complementary free energy and complementary dissipation potentials are assumed *a priori*. The specific forms selected here for both the Gibbs and complementary dissipation potentials result in a fully associative, multiaxial, isothermal, unified viscoplastic model with nonlinear kinematic hardening. Thus this model constitutes one of many models in the GVIPS (Generalized VIscoplasticity with Potential Structure) class of inelastic constitutive equations which can be constructed using the generalized framework of Arnold and Saleeb[1].

The particular unified GVIPS model of interest in this study possesses one tensorial internal state variable (i.e., the back or internal stress) that is associated with dislocation substructure and an evolutionary law that has nonlinear kinematic hardening and both thermal and strain induced recovery mechanisms. A unique aspect of the present model is the inclusion of non-linear hardening through the use of a compliance operator (derived from the Gibb's potential) in the evolution law for the back stress. This non-linear tensorial operator is significant in that it allows both the flow and evolutionary laws to be fully associative (and therefore easily integrated) [2] and greatly influences the multiaxial response under non-proportional loading paths [1],[3],[4]. In addition to this nonlinear compliance operator, a new consistent, potential preserving, internal unloading criterion has been introduced to prevent abnormalities in the predicted stress-strain curves, which are present with nonlinear hardening formulations, during unloading and reversed loading. This new criterion is motivated by considering the trajectory of the state point through the state space during unloading and hinges upon the introduction of internal state discontinuity inequalities for the conjugate back (or internal) strain rate.

A primary objective of the present study is to specify material functions and characterize the associated material parameters for the current kinematic, isothermal GVIPS model given TIMETAL 21S[1], an advanced titanium-based matrix commonly used in TMCs. Although both long and short term behavior is important, capturing the short term (or transient) behavior and rate sensitivity of the material is of primary importance given that the applications of interest are primarily those involving processing and propulsion systems. Furthermore, to illustrate the effectiveness of the present model a comparison of the GVIPS model and a particular Bodner-Partom (BP) model discussed in [5] (of the commonly used BP models [6]-[8] in the literature) is made on the basis of predictive accuracy and numerical efficiency.

The paper begins by briefly summarizing the complete potential structure, followed by a multiaxial and uniaxial statement of the newly proposed GVIPS model, including a discussion on the recent addition of a potential preserving internal unloading criterion. A discussion regarding the characterization of the proposed model is then followed by numerous results illustrating the predictive accuracy and numerical efficiency of the model.

3 Complete Potential Structure

Here the basic thermodynamic framework put forth by Arnold and Saleeb [1] is summarized. Expressions for the Gibb's thermodynamic and the complementary dissipation potential functions are assumed in

[1]TIMETAL 21S is a registered trademark of TIMET, Titanium Metals Corporation.

terms of a number of state and internal variables characterizing the changing internal structure of the material. For conciseness, the discussion is limited to a case involving i) small deformations (in which the initial state is assumed to be stress free throughout), ii) an initially isotropic material, iii) isothermal conditions, and iv) the specialized potential framework discussed in [1]. A Cartesian coordinate reference frame and index notation are utilized (repeated Roman subscripts imply summation).

Given the Gibb's potential in the following form

$$\Phi = \Phi(\sigma_{ij}, \alpha_\gamma, T, \epsilon^I_{ij}) \tag{1}$$

and assuming *a priori* that the inelastic strain is an independent parameter (and not an internal state variable), for example

$$\Phi = \bar{E}(\sigma_{ij}) - \sigma_{ij}\epsilon^I_{ij} + \bar{H}\,(\alpha_\gamma) - Z(T) - \frac{\sigma_{kk}}{3}\eta(T - T_o), \tag{2}$$

an expression for the total strain rate can be obtained by differentiating, that is,

$$\dot{e}_{ij} = \frac{d}{dt}\left(\frac{-\partial\Phi}{\partial\sigma_{ij}}\right) = C_{ijrs}\dot{\sigma}_{rs} + \dot{\epsilon}^I_{ij} + \delta_{ij}\frac{\eta}{3}\dot{T} \tag{3}$$

as well as the rate of change of the conjugate internal variables (A_ξ),

$$\dot{A}_\xi = \frac{d}{dt}\left(\frac{-\partial\Phi}{\partial\alpha_\xi}\right) = Q_{\xi\gamma}\dot{\alpha}_\gamma \tag{4}$$

where

$$C_{ijrs} = \frac{-\partial^2\Phi}{\partial\sigma_{ij}\partial\sigma_{rs}} = \frac{-\partial^2\bar{E}(\sigma_{ij})}{\partial\sigma_{ij}\partial\sigma_{rs}} \tag{5}$$

$$Q_{\xi\gamma} = \frac{-\partial^2\Phi}{\partial\alpha_\xi\partial\alpha_\gamma} = \frac{-\partial^2\,\bar{H}\,(\alpha_\gamma)}{\partial\alpha_\xi\partial\alpha_\gamma} \tag{6}$$

are the external and internal compliance operators, respectively. Note the three terms in equation (3) may then be identified as the reversible, irreversible (inelastic), and thermal expansion components of the total strain rate, respectively. Thus,

$$\dot{e}_{ij} = \dot{\epsilon}^R_{ij} + \dot{\epsilon}^I_{ij} + \dot{\epsilon}^T_{ij} \tag{7}$$

where

$$\dot{\epsilon}^R_{ij} = C_{ijrs}\dot{\sigma}_{rs} \tag{8}$$

and

$$\dot{\epsilon}^T_{ij} = \delta_{ij}\frac{\eta}{3}\dot{T} \tag{9}$$

but $\dot{\epsilon}^I_{ij}$ (the inelastic strain rate) is defined separately using the concept of a dissipation potential $\Omega(\sigma_{ij}, \alpha_\gamma, T)$.

Given

$$\Omega = \Omega(\sigma_{ij}, \alpha_\gamma, T) \tag{10}$$

and using the Clausius-Duhem inequality; the flow law becomes

$$\dot{\epsilon}^I_{ij} = \frac{\partial\Omega}{\partial\sigma_{ij}} \tag{11}$$

and the evolutionary laws for the thermodynamic conjugate internal state variables:

$$\dot{\mathcal{A}}_\gamma = -\frac{\partial \Omega}{\partial \alpha_\gamma} \tag{12}$$

Utilizing equation (4) the internal constitutive rate equations for the internal state variables is obtained,

$$\dot{\alpha}_\gamma = L_{\gamma\xi}\, \dot{\mathcal{A}}_\xi \tag{13}$$

where

$$L_{\gamma\xi} = [Q_{\gamma\xi}]^{-1} = \left[\frac{-\partial^2 \Phi}{\partial \alpha_\xi \partial \alpha_\gamma}\right]^{-1} \tag{14}$$

Thus, equations (11) and (12) represent the flow and evolutionary laws, for an assumed $\Omega = \Omega(\sigma_{ij}, \alpha_\gamma, T)$, and equation (13) the internal constitutive rate equations, given a Gibb's potential Φ, wherein both potentials are directly linked through the internal state variables α_γ.

4 Viscoplastic Constitutive Model

A complete multiaxial statement of a GVIPS model can be derived by using the above framework, given a specific form for both the Gibb's potential, Φ, and the complementary dissipation potential, Ω. Form invariance (objectivity) of these potentials requires that they depend only on certain invariants of their respective tensorial arguments (*i.e.*, an integrity basis [9]). In the spirit of von Mises and because of the deviatoric nature of inelastic deformation, only the quadratic invariant will be considered at this time in specifying the dissipation potential. Similarly, only the linear elastic strain energy contribution will be considered in specifying the Gibb's potential, with the internal state groupings being functions of the respective quadratic invariants. Finally, although equation (10) indicates that an unlimited number of internal state variables can be specified, here our attention will be restricted to a GVIPS model with a single *independent*, evolving, internal state variable. This internal state variable, a_{ij}, is taken to be a second order symmetric traceless tensor that represents the internal (or back) stress associated with dislocation substructure. Two additional scalar state variables, one representing the drag strength (κ) and taken to be non-evolving and the other a yield stress (Y) that is uniquely assumed to implicitly evolve with internal stress are considered. Both variables are associated with dislocation density and are included in anticipation of the subsequent nonisothermal GVIPS model. However, in the forthcoming nonisothermal formulation κ will explicitly be taken as an evolving internal state variable with its own associative evolution law (see [3]).

Consequently, the Gibb's potential may be written as

$$\Phi = -\frac{1}{2} C_{rskl}\sigma_{rs}\sigma_{kl} - \sigma_{ij}\epsilon^I_{ij} + H_1(G) - Z(T) - \frac{\sigma_{kk}}{3}\eta(T - T_o) \tag{15}$$

and the dissipation potential as

$$\Omega = \mu \int f(F)dF + R_\alpha B_0 \int g(G)dG \tag{16}$$

where

$$F = \left\langle \frac{\sqrt{J_2}}{\kappa} - Y \right\rangle \tag{17}$$

$$Y = \left\langle 1 - \beta\sqrt{G} \right\rangle \tag{18}$$

$$G = \frac{I_2}{\kappa^2} \tag{19}$$

$$H_1(G) = -B_0(G + B_1 G^p) \tag{20}$$

$$I_2 = \frac{3}{2} a_{ij} a_{ij} \tag{21}$$

$$J_2 = \frac{3}{2} \Sigma_{ij} \Sigma_{ij} \tag{22}$$

$$\Sigma_{ij} = S_{ij} - a_{ij} \tag{23}$$

$$S_{ij} = \sigma_{ij} - \frac{1}{3} \sigma_{kk} \delta_{ij} \tag{24}$$

$$a_{ij} = \alpha_{ij} - \frac{1}{3} \alpha_{kk} \delta_{ij}. \tag{25}$$

Note that in the preceding expression for the dissipation potential, the stress dependence, both external and internal, enters through the scalar functions F and G in the form of effective (Σ_{ij}) and internal (a_{ij}) deviatoric stresses, respectively. Furthermore, the function F acts like a threshold surface, because when $F < 0$, no inelastic strain can occur. Clearly, this threshold value is dictated by the magnitude of both the drag strength (κ) and yield stress (Y). A unique aspect of this model is that the internal variable representing the yield stress is specifically taken as a special scaled function of the back stress and drag strength. Consequently, this allows for 1) the model to possess features of a model with three internal variables yet without any additional computational cost, and 2) the presence of an induced strain recovery term (as opposed to the common 'ad-hoc' introduction of such terms) in the evolution of the back strain (i.e., the associated conjugate variable, $\mathcal{A}_\gamma$). It is important to realize that the product κY constitutes the radius of the initial threshold surface (see Fig 1a), thereby dictating from physical arguments, that both Y and κ be always positive valued. Furthermore, given the specified form of Y in equation (18), it is clear that the material parameter ratio (β/κ) will dictate the limit value (i.e., when Y=0) of the internal stress (α_{ij}), or the cut-off limit for dynamic recovery.

By selecting the preceding scalar functions, a general yet *complete* potential-based model, with *associated* flow and evolutionary laws can be constructed. The second invariants , J_2 and I_2 , are also scaled for tension. These invariants could just as easily have been scaled for shear by replacing the coefficient 3/2 with 1/2, and modifying the definition of the magnitude of the inelastic strain rate that follows. Also, it should be stated that the linear form of F and Y in equations (17) and (18) was chosen in order to allow algebraic manipulation and analytical solution of the resulting expressions (e.g., inversion of the flow law), so as to ease the characterization stage of the model, as discussed subsequently in sections 4.1 and 4.2. Note, however, that the quadratic form of F and Y does provide some additional interesting features in the model as discussed previously by Arnold et al. [3].

Finally, it is interesting to note the close similarity between the present assumed form of the threshold surface F of equation (14) to that used by Lemaitre and Chaboche [13] in the context of inviscid plasticity. The significant difference between the two forms is that Lemaitre and Chaboche [13] utilized a non-associated format; the form similar to equation (14) was taken to affect only the directions of inelastic and internal state, whereas a classical J_2 form was employed to control yielding (*i.e.*, the consistency condition). In the present fully associative case, the same threshold surface F is used to affect both yielding, and the direction of inelastic and internal state.

Taking the appropriate derivatives of both Φ and Ω as indicated in equations (2) through (14), one obtains the multiaxial isothermal specification particular to the present constitutive model. Here the decomposition of the total strain rate is that of equation (7), where the reversible strain rate is given by equations (8) and (9) and the irreversible (or inelastic) component is defined by the following flow law:

$$\dot{\epsilon}^I_{ij} = \frac{3}{2} ||\dot{\epsilon}^I_{ij}|| \frac{\Sigma_{ij}}{\sqrt{J_2}} \qquad if \quad F \geq 0 \tag{26}$$

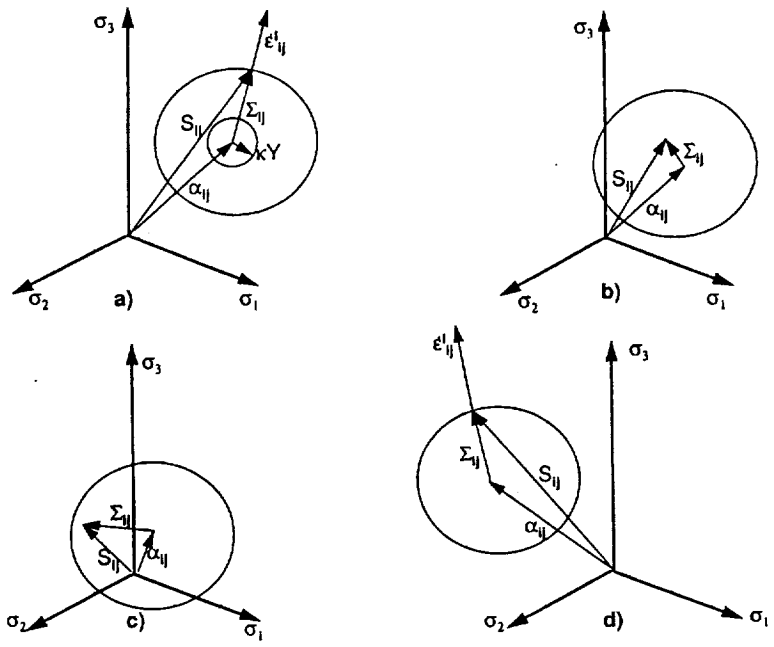

Figure 1: Geometric interpretation of the internal unloading criterion relative to positions of the threshold surfaces.

or

$$\dot{\epsilon}^I_{ij} = 0 \qquad if \quad F < 0 \tag{27}$$

where

$$||\dot{\epsilon}^I_{ij}|| = \sqrt{\frac{2}{3}\dot{\epsilon}^I_{ij}\dot{\epsilon}^I_{ij}} = \frac{\mu f(F)}{\kappa} \tag{28}$$

The internal constitutive rate equation is always given by

$$\dot{a}_{ij} = L_{ijrs}\,\dot{\mathcal{A}}_{rs} \tag{29}$$

while the evolutionary law for the back strain rate is given by :

$$\dot{\mathcal{A}}_{kl} = \dot{\epsilon}^I_{kl} - \frac{3}{2}\frac{\beta}{\kappa}||\dot{\epsilon}^I_{ij}||\frac{a_{kl}}{\sqrt{G}}Hv[Y] - \frac{3R_\alpha B_0\; g(G)}{\kappa^2}a_{kl} \qquad if \quad a_{ij}\Sigma_{ij} \geq 0 \tag{30}$$

during internal loading and

$$\dot{\mathcal{A}}_{rs} = Q_{rslm}E_{lmnp}\left(\dot{\epsilon}^I_{np} - \frac{3}{2}\frac{\beta}{\kappa}||\dot{\epsilon}^I_{ij}||\frac{a_{np}}{\sqrt{G}}Hv[Y] - \frac{3R_\alpha B_0\; g(G)}{\kappa^2}a_{np}\right) \qquad if \quad a_{ij}\Sigma_{ij} < 0 \tag{31}$$

during internal unloading, as indicated by the inequality $a_{ij}\Sigma_{ij} < 0$. The internal stiffness operator is defined as

$$L_{ijrs} = [Q_{ijrs}]^{-1} = \frac{\kappa^2}{3B_0(1+B_1pG^{p-1})}\left(I_{ijrs} - \frac{3B_1(p-1)G^{p-2}}{\kappa^2(1+B_1pG^{p-1}(6p-5))}a_{rs}a_{ij}\right) \tag{32}$$

with $I_{ijrs} = \delta_{ir}\delta_{js}$.

Equation 31 constitutes a new consistent, potential preserving, internal unloading criterion that will prevent the classical abnormalities [13] in the cyclic response associated with nonlinear hardening formulations, upon unloading and reversed loading of the *external* variables. This new criterion is motivated by considering the trajectory of the state point within the state space during unloading and hinges upon the introduction of an internal state discontinuity inequality for the conjugate internal (or back) strain rate. Mathematically, this is accomplished by the introduction of a dissipation potential that is distinctly different when the material is undergoing internal loading versus unloading. The geometric interpretation of this criterion (discontinuity inequality) in the $\pi-$ plane is illustrated in Fig. 1, where the situation of the deformed material $a_{ij} \neq 0$, is depicted. Note that the projection of the applied stress vector σ_{ij} on the $\pi-$ plane is, of course, S_{ij} , the deviatoric stress and that the projection of the cylindrical surfaces of constant inelastic strain rate (F=constant) appear as concentric circles in this plane, although only one is illustrated in Fig. 1. The current effective stress vector $\Sigma_{ij} = S_{ij} - a_{ij}$ emanates from the translated center of the nested circles and the corresponding inelastic strain rate vector $\dot{\epsilon}^I_{ij}$, is collinear with it. Now, if the applied stress is reduced to a value less than the internal stress, the effective stress will change sign and unloading internal to the material will take place, thus resulting in a readjustment (state recovery, i.e., shift toward the origin of the $\pi-$ plane) in internal stress a_{ij} as shown in Fig. 1b. If the stress reversal were continued, the material would also continue to rapidly readjust until once again internal reloading commenced, as depicted in Fig. 1c.

Justification for this criterion stems from the work of Orowan [14] and others, and has indicated that upon stress reversals dislocations are remobilized and consequently rapid rearrangement of these dislocations is possible within the wake of the previous load path. To describe this rapid motion of dislocation remobilization (readjustment of internal stress) during material unloading we introduce, in the spirit of Robinson [15] and Onat [11] , distinct regions within the state space in which the *rate* of the conjugate internal state variable (internal strain) changes discontinuously. Currently, until more exploratory tests can be performed to fully describe the affected regions of the state space, the internal (back) strain rate during internal unloading is taken to be proportional to the back strain rate during loading, through the product of the external stiffness and internal compliance operators, see eq. (30). Thus, implying that the internal stress and strain during internal unloading are related by the external stiffness tensor; the accuracy of such an assumption can be verified by conducting a number of transient stress dip tests [10]. Furthermore, an examination of the evolution of the conjugate of the internal stress (*i.e.*, the internal strain, $\mathcal{A}_{ij}$), clearly shows that equation (30) possesses, as typically assumed in the literature [17], [18] competitive mechanisms consisting of a hardening term (which accounts for strengthening mechanisms) and two state recovery terms (which account for softening mechanisms). The first state recovery term evolves with inelasticity; it is strain induced, and is commonly called dynamic recovery; whereas, the second term, interchangeably called static or thermal recovery, evolves with time and is thermally induced. Again, it is important to note that as the internal stress evolves and finally reaches a limit value (dictated by the material parameters β and κ) the yield stress will vanish, as will the strain induced recovery term. The added flexibility provided by the dynamic recovery term is particularly advantageous under conditions where thermal recovery is relatively small (i.e., low homologous temperatures).

Finally, the above expressions are further specialized by assuming the nonlinearity of inelasticity and the thermal recovery process to be represented by power law functions, that is:

$$f(F) = F^n \tag{33}$$

$$g(G) = G^q \tag{34}$$

4.1 Uniaxial Simplification and State Space Representation

If we consider only a uniaxial state of stress, the deviatoric applied and internal stress tensors become

$$S_{ij} = \frac{1}{3}\begin{bmatrix} 2\sigma & 0 & 0 \\ 0 & -\sigma & 0 \\ 0 & 0 & -\sigma \end{bmatrix}$$

and

$$a_{ij} = \frac{1}{3}\begin{bmatrix} 2\alpha & 0 & 0 \\ 0 & -\alpha & 0 \\ 0 & 0 & -\alpha \end{bmatrix}$$

such that

$$F = \left\langle \frac{\sigma - \alpha}{\kappa} - Y \right\rangle \tag{35}$$

$$Y = \left\langle 1 - \beta\frac{\alpha}{\kappa} \right\rangle \tag{36}$$

$$G = \frac{\alpha^2}{\kappa^2}$$

and the flow and evolutionary laws, respectively, become

$$\dot{\epsilon}^I = \frac{\mu}{\kappa} F^n \frac{(\sigma - \alpha)}{|\sigma - \alpha|} \tag{37}$$

and

$$\dot{\alpha} = \frac{3}{2}\mathcal{H}(1 - \frac{2}{3}\mathcal{C}\alpha^2)\left\{\dot{\epsilon}^I - \beta \parallel \dot{\epsilon}^I \parallel Hv[Y]\alpha - \frac{2R_\alpha B_0}{\kappa}\left(\frac{\alpha}{\kappa}\right)^{2q+1}\right\} \qquad if \quad (\sigma - \alpha)\alpha \geq 0 \tag{38}$$

$$\dot{\alpha} = -3\hat{G}\left\{(1 + \beta\alpha Hv[Y]) \parallel \dot{\epsilon}^I \parallel + \frac{2R_\alpha B_0}{\kappa}\left(\frac{\alpha}{\kappa}\right)^{2q+1}\right\} \qquad if \quad (\sigma - \alpha)\alpha < 0 \tag{39}$$

Utilizing the concept of the state space representation [10] through [12], we can examine and illustrate geometrically the various features of the present unified viscoplastic model and discuss its characterization. The pertinent state space is constructed by combining and rewriting equations (7), (37), and (38), in standard vector form as follows, and plotting the corresponding $\dot{\mathcal{G}}$ fields or relaxation trajectories. That is,

$$\dot{\mathcal{S}} = \dot{\mathcal{G}}\,(\sigma, \alpha) + \dot{\mathcal{D}}\,(\dot{e})$$

or, for example, during loading,

$$\begin{Bmatrix} \dot{\sigma} \\ \dot{\alpha} \end{Bmatrix} = \begin{Bmatrix} -\hat{E}\,\dot{\epsilon}^I \\ \frac{3}{2}\mathcal{H}(1 - \frac{2}{3}\mathcal{C}\alpha^2)\left[\dot{\epsilon}^I - \beta \parallel \dot{\epsilon}^I \parallel Hv[Y]\alpha - \frac{2R_\alpha B_0}{\kappa}\left(\frac{\alpha}{\kappa}\right)^{2q+1}\right] \end{Bmatrix} + \begin{Bmatrix} \hat{E}\,\dot{e} \\ 0 \end{Bmatrix} \tag{40}$$

where

$$\parallel \dot{\epsilon}^I \parallel = \frac{\mu}{\kappa} F^n \tag{41}$$

$$\mathcal{H} = \frac{\kappa^2}{3B_0(1 + B_1 p\left(\frac{\alpha}{\kappa}\right)^{2p-2})} \tag{42}$$

$$\mathcal{C} = \frac{3B_1(p-1)\left(\frac{\alpha}{\kappa}\right)^{2p-4}}{\kappa^2(1 + B_1 p\left(\frac{\alpha}{\kappa}\right)^{2p-2}(6p-5))} \tag{43}$$

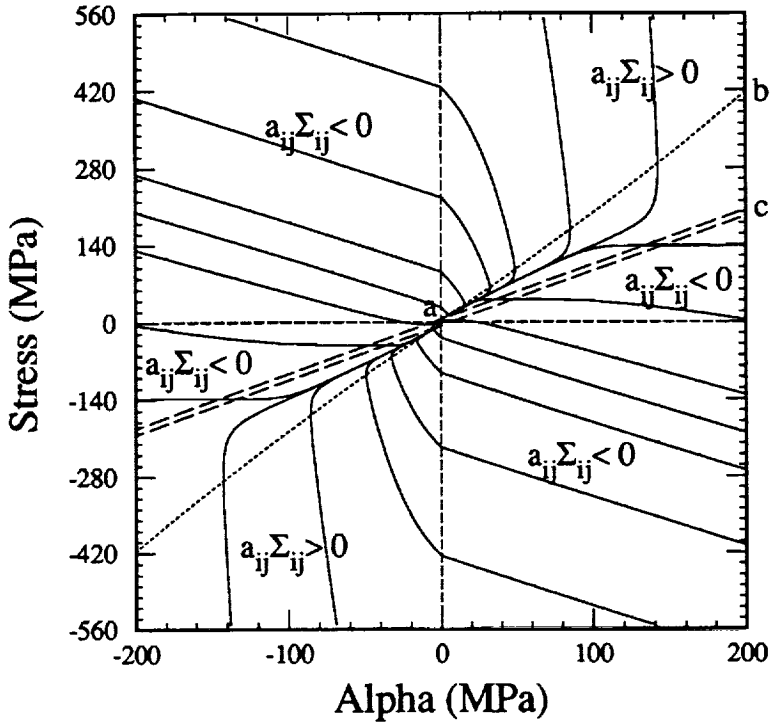

Figure 2: State space associated with the material parameters in Table 1.

and $\dot{e}$ is the total uniaxial strain rate. These relaxation trajectories are obtained from equations (37) and (40) by imposing a constant total strain rate (*i.e.*, $\dot{e}= 0$), thereby implying that $\dot{\mathcal{S}}=\dot{\mathcal{G}}\ (\sigma, \alpha)$.

Figure 2 illustrates the state space representation associated with equations (37), (38) and (39), and the material parameters given in Table 1. Immediately, a number of qualitative features of the first and third quadrants of the state space can be deduced from equations (37) and (40). For example, the locus of steady state (or *fixed*) points in creep, denoted by line *ab* in Fig. 2 is obtained by imposing the condition $\dot{\mathcal{S}}= 0$ on equations (40). Mathematically, such a condition is obtained when

$$\sigma = (1 - \beta H v[Y])\alpha + \kappa \left[1 + \left[\frac{2R_\alpha B_0}{\mu(sgn(\dot{\epsilon}^I) - \beta H v[Y]\alpha)} \left(\frac{\alpha}{\kappa}\right)^{2q+1}\right]^{\frac{1}{n}}\right] \tag{44}$$

and is denoted as the locus of steady state creep. The associated steady state creep rate is

$$\dot{\epsilon}^I = \frac{\frac{2R_\alpha B_0}{\kappa} \left(\frac{\alpha}{\kappa}\right)^{2q+1}}{(sgn(\dot{\epsilon}^I) - \beta H v[Y]\alpha)} \tag{45}$$

Secondly, the locus of maxima in stress (*i.e.*, $\dot{\sigma} = 0$) during relaxation ($\dot{e} = 0$) occurs when

$$\dot{\epsilon}^I = -\frac{\dot{\sigma}}{\hat{E}} = 0 \tag{46}$$

This is satisfied when

$$\sigma = \kappa + \alpha(1 - \beta H v[Y]) \tag{47}$$

and is denoted by line *ac* in Fig. 2. The points on lines *ac* do not correspond to fixed points in the state space, as do those associated with line *ab*, since the internal stress continues to evolve, that is,

Constants	Units	TIMETAL 21S
Viscoplastic		
κ	MPa	5.86
μ	MPa/sec	$5.52\text{x}10^{-9}$
n	-	3.3
B_0	MPa	$5.86\text{x}10^{-4}$
B_1	-	0.05
p	-	1.8
q	-	1.35
R_α	1/sec	$0.1\text{x}10^{-5}$
β	-	0.01
Elastic		
$\hat{E}$	MPa	80,671
ν	-	0.3

Table 1: Isothermal material parameters for TIMETAL 21S at 650°C

$$\dot{\alpha} = -\frac{3}{2}\mathcal{H}(1-\frac{2}{3}\mathcal{C}\alpha^2)\left\{\frac{2R_\alpha B_0}{\kappa}\left(\frac{\alpha}{\kappa}\right)^{2q+1}\right\} \tag{48}$$

Note that the inelastic strain is zero along and within the zone denoted by line ac, as in this region $F < 0$. Finally, Fig. 2 illustrates clearly that the second and fourth quadrants as well as the lower portions of quadrants one and three contain distinctly different relaxation trajectories resulting from the imposition of the internal unloading criterion.

4.2 Characterization

The most important, and often times most difficult, aspect of modeling the behavior of a given material at elevated temperature is obtaining the required material functions, e.g., f(F) and g(G), and material parameters. The difficulty associated with this process typically stems from not only the variety in mathematical forms for the material functions (e.g., power law, exponential, hyperbolic sine, etc.), but also the fact that given the material functions there is not a unique set of material parameters for any given load path. Therefore, numerous iterations and difficult compromises are required before a final set of material parameters, for the assumed material functions, can be obtained.

With the present isothermal GVIPS model, nine material parameters need to be determined, as given in Table 1: three are associated with the flow law (i.e., κ, μ, and n); three with the nonlinear hardening operator, (i.e., B_0, B_1, and p); two with the internal thermal recovery term (i.e., R_α and q); and one with the dynamic recovery term (i.e., β). Both elastic and inelastic material parameters given in Table 1 correspond to the reference temperature (T_{ref}) of 650°C. This temperature was chosen as the reference temperature because at 650°C the material exhibits cyclically neutral behavior and thus supports the use of a purely kinematic model. Here a brief outline of the characterization process is given, with a more complete discussion regarding both exploratory and characterization testing given by Arnold [10] and Castelli et al. [19]. All tests addressed are uniaxial isothermal experiments, thus implying that the multiaxial material constants are typically generalized from their uniaxial counterparts. This need for generalization is precisely why a consistent multiaxial theory, such as that developed from a potential formulation, is imperative. The available tests for use in characterizing the current model are, three relaxation tests, three creep tests, one multiple-step creep test, and three tensile curves at different total strain rates.

Initially, the yield stress is unity and therefore the radius of the threshold surface is determined by the drag strength and represents that value of stress below which only elastic behavior is "observed",

i.e., no measurable inelastic behavior occurs. The actual numerical value employed will obviously be non-unique as it will be dependent upon the sensitivity of the experimental equipment and/or definition of inelasticity employed. A preferred approach to arrive at a value for κ is to conduct a sequence of creep or relaxation probing tests to determine the maximum value of stress for which no time dependent behavior ($\dot{\epsilon}^I = 0$) is observed. An alternative approach and the one taken here (given the availability of three relaxation test results) is to use the minimum stress value attained at the end of a 24 hour period as our maximum allowable drag strength (i.e., $\kappa \leq 7$ MPa) since all relaxation trajectories in the state space tend toward the origin (i.e., $\sigma = \kappa$, $\alpha = 0$, see Fig. 2).

Given κ and taking $\beta \approx 0$ (because at T_{ref} the thermal recovery mechanism dominates) the material parameters μ and n may be obtained from either variable strain rate tests or stress transient dip tests, as discussed in Arnold [10]. Here, given a multiple step creep test which is a type of variable strain rate test, data pairs can be obtained at the beginning and end of each step in stress, e.g., $(\sigma_1, \dot{\epsilon}_1^I)$, $(\sigma_2, \dot{\epsilon}_2^I)$, respectively. Assuming that the internal stress α is equal to α^* both before and after the step in stress (i.e., points 1 and 2) the following relation may be obtained from eliminating α^* from the corresponding flow laws at points 1 and 2 (see equation (36)); that is,

$$\left[\frac{\sigma_1 - \sigma_2}{\kappa}\right] = \left(\frac{\kappa}{\mu}\dot{\epsilon}_1^I\right)^{\frac{1}{n}} - \left(\frac{\kappa}{\mu}\dot{\epsilon}_2^I\right)^{\frac{1}{n}} \tag{49}$$

where the only unknowns are μ and n. Employing a sufficient number of data pairs and a nonlinear regression scheme, optimal values for μ and n can be found.

Next, assuming that hardening dominates the early portion of a creep test (primary creep stage) the thermal recovery term in the evolutionary law may be neglected. Consequently, the internal stress rate of equation (38) can be expressed as

$$\dot{\alpha} = \frac{3}{2}\mathcal{H}(1 - \frac{2}{3}\mathcal{C}\alpha^2)\dot{\epsilon}^I \tag{50}$$

given that $\beta \approx 0$. Furthermore, an expression for $\dot{\alpha}$ in terms of $\dot{\epsilon}^I, \ddot{\epsilon}^I, \dot{\sigma}$, and α can be obtained from differentiation of the flow law in equation (37), that is,

$$\dot{\alpha} = \frac{\dot{\sigma} - \frac{\kappa^2}{\mu n}\left(\ddot{\epsilon}^I + \frac{2\dot{\epsilon}^I|\dot{\sigma}|}{(\sigma-\alpha)}\right)\left(\frac{\kappa}{\mu}\dot{\epsilon}^I\right)^{\frac{(1-n)}{n}}}{\left[1 + \frac{\kappa^2}{\mu n}\frac{2\dot{\epsilon}^I}{(\sigma-\alpha)}\left(\frac{\kappa}{\mu}\dot{\epsilon}^I\right)^{\frac{(1-n)}{n}}\right]} \tag{51}$$

Thus, equating equation (50) and (51), assuming that κ, μ, and n are known, considering data pairs $(\sigma, \epsilon^I, \dot{\epsilon}^I, \ddot{\epsilon}^I, \alpha)$ taken from primary creep data, and using again a nonlinear regression scheme, the material parameters B_0, B_1, and p can be determined. Given multiple creep curves a number of sets of B_0, B_1, and p may be obtained and then a weighted averaged can be computed to give a single optimum set.

Finally, the material parameters associated with thermal recovery (R_α and q) may be determined using the data pairs $(\sigma_s, \dot{\epsilon}_s^I)$ associated with the constant strain rate portion of the creep curve, and the corresponding internal stress (that is calculated from the flow law) at this assumed steady state (α_s),

$$\alpha_s = \frac{\sigma_s - \kappa\left[1 + \left(\frac{\kappa}{\mu}\dot{\epsilon}_s^I\right)^{\frac{1}{n}}\right]}{1 - \beta H v[Y]} \tag{52}$$

Upon obtaining these data pairs, one may take the natural logarithm of both sides of equation (45) and determine R_α and q from the ordinate intercept and slope, respectively, of the resulting ln-ln plot.

The above outlined procedure can easily be applied to obtained an initial set of required material parameters. This set must, however, be further optimized to obtain a final set of material parameters

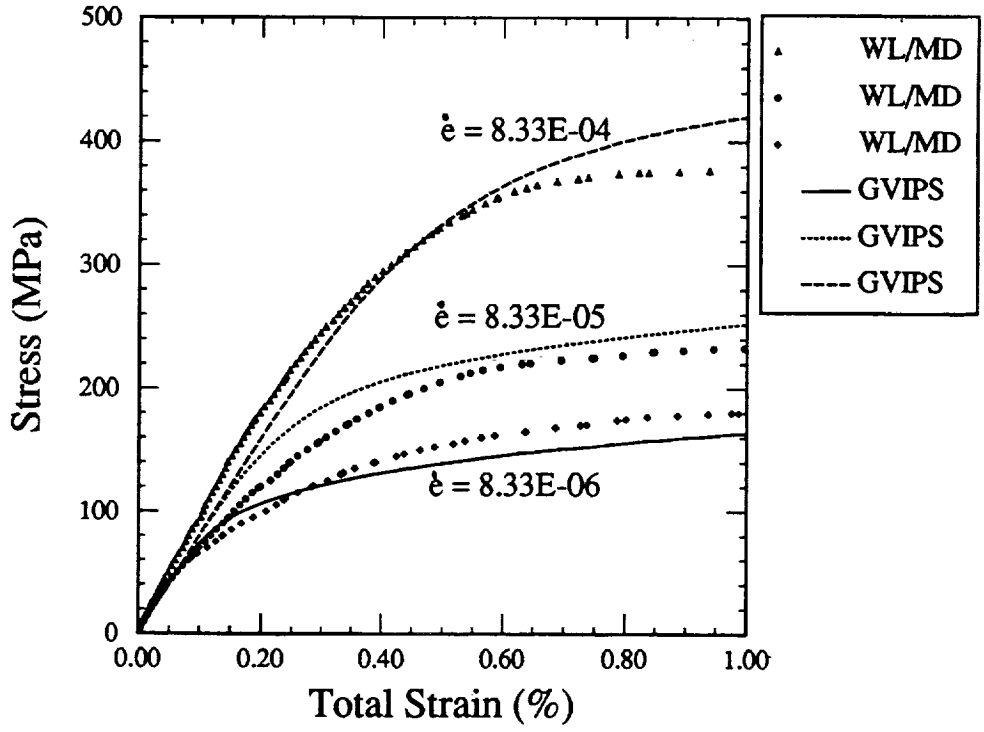

Figure 3: GVIPS correlation with experimental tensile data [18] considering the effect of strain rate.

that will allow accurate correlation of the model over a "wide range of loading". In the present case, the authors are primarily interested in the short term response ($\leq 7200s$) and small strain ($\approx 1\%$) regime of the titanium alloy TIMETAL 21S. The resulting optimized material parameter set for TIMETAL 21S is given in Table 1.

The corresponding correlation for, 1) the tensile response of TIMETAL 21S over three orders of magnitude in total strain rate (i.e., $\dot{e} = 8.33\text{x}10^{-4}, 8.33\text{x}10^{-5}, 8.33\text{x}10^{-6}$) , 2) short term creep at three stress levels (i.e., σ = 72, 110, and 128 MPa), and 3) relaxation at 238 MPa are shown respectively in Figs. 3, 4 and 5, wherein the symbols denote experimental data and the lines the model correlations. In the authors' opinions the model does a very good job, given a single set of constants, for the wide variety of loading conditions examined. It is important to remind the reader that if one were to focus on only one type of loading condition, superior correlations could be achieved for that class of loading; however, predictions of other classes of loading would severely suffer. For example during the above characterization process excellent tensile correlation was obtained but at the expense of poor creep and relaxation behavior for a given set of material parameters. Conversely, when the model was calibrated for creep response poor tensile and relaxation behavior were similarly predicted.

5 GVIPS Predictions

The present GVIPS model, characterized to represent the behavior of TIMETAL 21S at 650°C, is now exercised and its predictive capability assessed. The assessment begins by considering relaxation tests performed at stress levels above and below that used in the characterization of the model. The corresponding short term (i.e., $\leq 800s$) and mid term (i.e., $\leq 7200s$) relaxation responses are shown in Figs. 5 and 6, respectively. Again, it is apparent that overall agreement with short term behavior is good while that of mid term is only reasonable. Note how the initial stress rates are accurate at the higher stress levels and yet diminish more rapidly than do the actual experimental values.

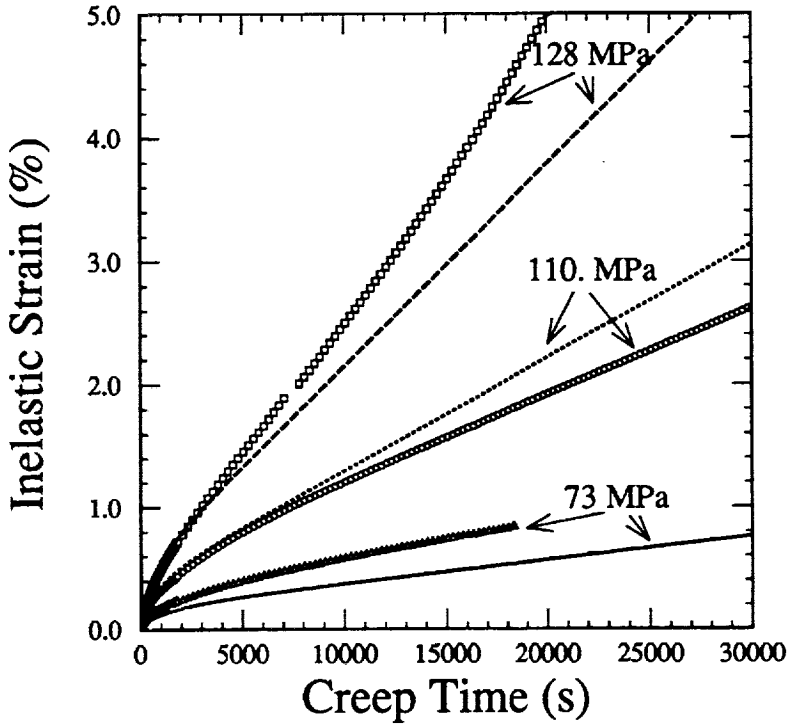

Figure 4: GVIPS correlation with experimental data of TIMETAL 21S under creep.

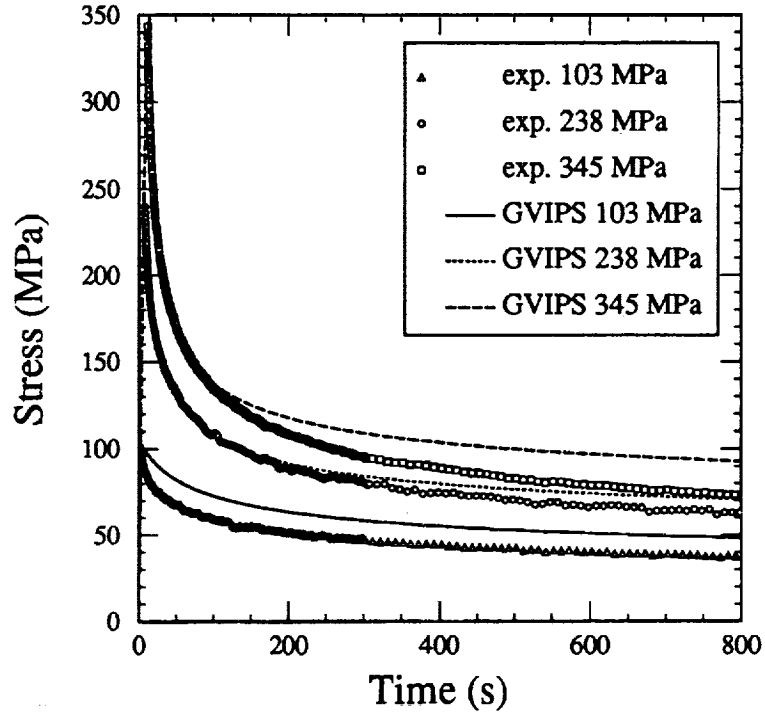

Figure 5: Short term relaxation response of TIMETAL 21S: GVIPS simulation versus experimental results.

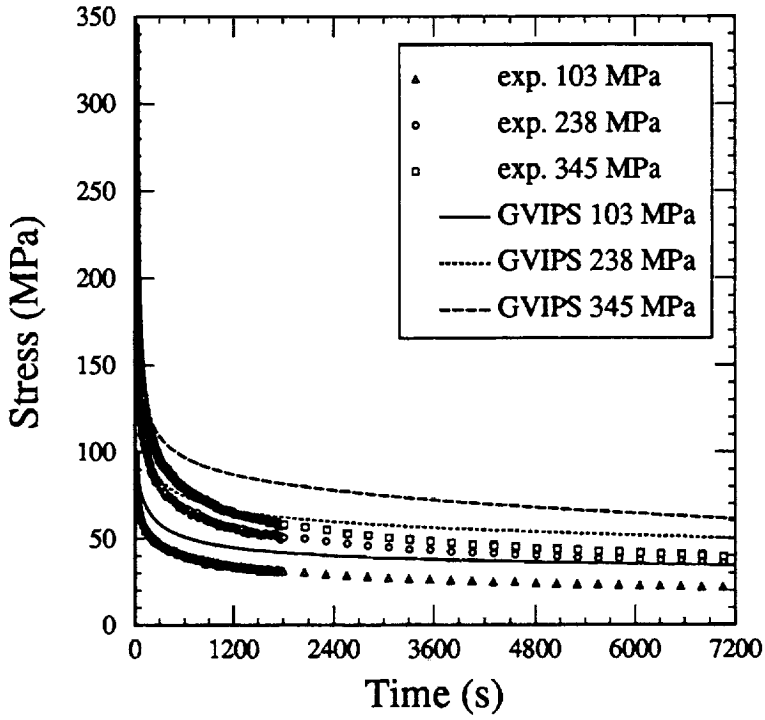

Figure 6: Mid term relaxation response of TIMETAL 21S: GVIPS simulation versus experimental results.

Figure 7 illustrates the cyclic behavior under strain control given a total strain rate of 8.33×10^{-5}, wherein the symbols represent the experimental results and the solid line the GVIPS prediction. Again, the agreement is adequate with approximately a 20% over-prediction of the maximum stress at ± 0.01 strain. Although not shown in Fig. 7, note that two cycles are required with the GVIPS model before the hysteresis loop will close.

A multiple step creep test is considered next, where the resulting inelastic strain versus time (at constant stress) is shown in figure 8. Here the GVIPS (solid line) simulation is seen to significantly under-predict, the accumulated inelastic strain as compared with the experimental data (denoted by the symbols). This is not surprising, however, given the fact that the model under-predicts the creep behavior at 72 MPa (see Fig. 4) and that this test was performed under constant load and not constant stress as was the simulation. As a consequence of the constant load controlled creep test, the experimental results have both additional geometric effects and possibly creep damage (thereby leading to tertiary creep) included in them. Neither of these factors have been included in the numerical simulation. The influence of these factors is particularly evident during the third step, where the inelastic strain rate during the experiment is significantly greater than that simulated (cf. $\sigma = 128$ MPa in Fig. 4).

Lastly, a classic plasticity-creep interaction experiment was performed and simulated to illustrate the need for a unified viscoplastic formulation. Here the material is subjected to an overload prior to performing a creep test at a lower stress value, as shown in Fig. 9. Typically, as is found here, the initial creep response following the overload is significantly reduced when compared to that produced from a pure creep test at this lower stress amplitude, see Fig. 10. Once again comparing the numerical simulation (of the GVIPS model) to that of the experimental results one observes reasonable overall agreement. Although, the amount of total accumulated creep strain at the end of the test, i.e., 72000 seconds, is significantly under estimated, the initial reduction in primary creep rate, due to the overload, is extremely accurate during the first 800 seconds and good over the first hour of creep loading, thus fulfilling our primary objective.

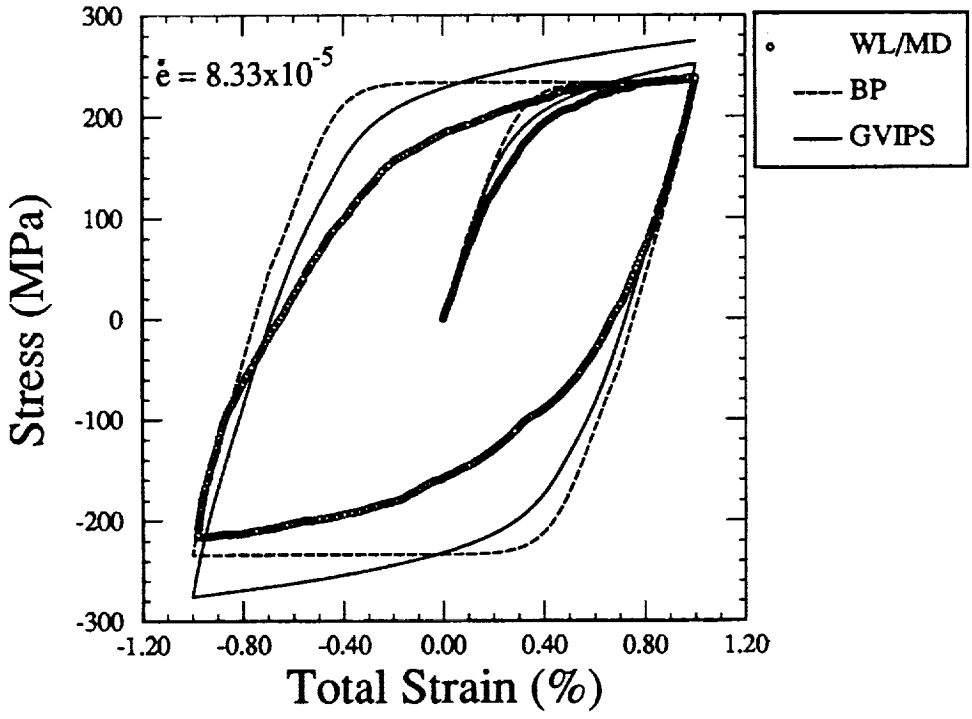

Figure 7: GVIPS and BP simulations versus cyclic behavior of TIMETAL 21S [18].

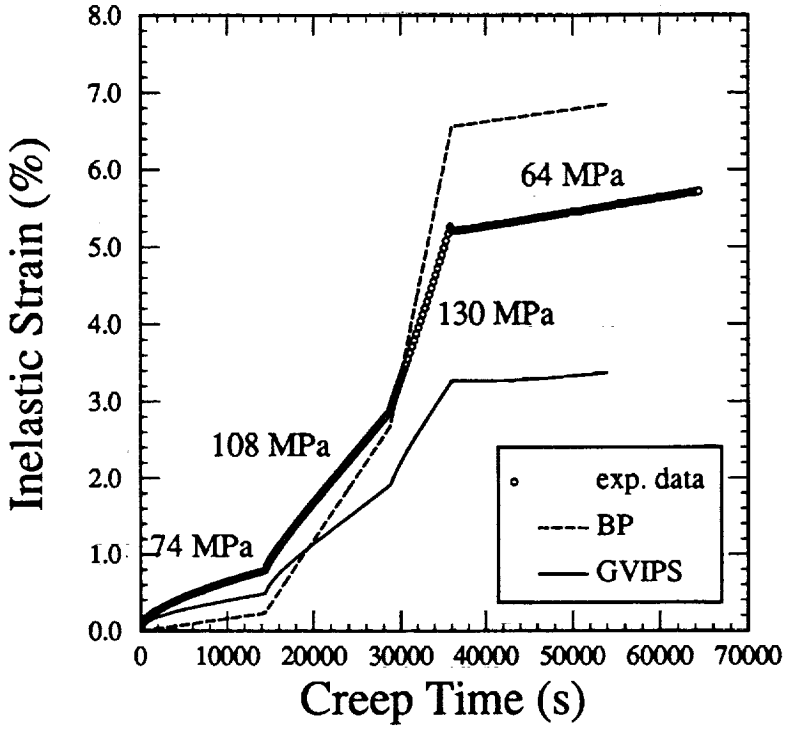

Figure 8: Multistep creep test: GVIPS and BP simulations versus experimental data

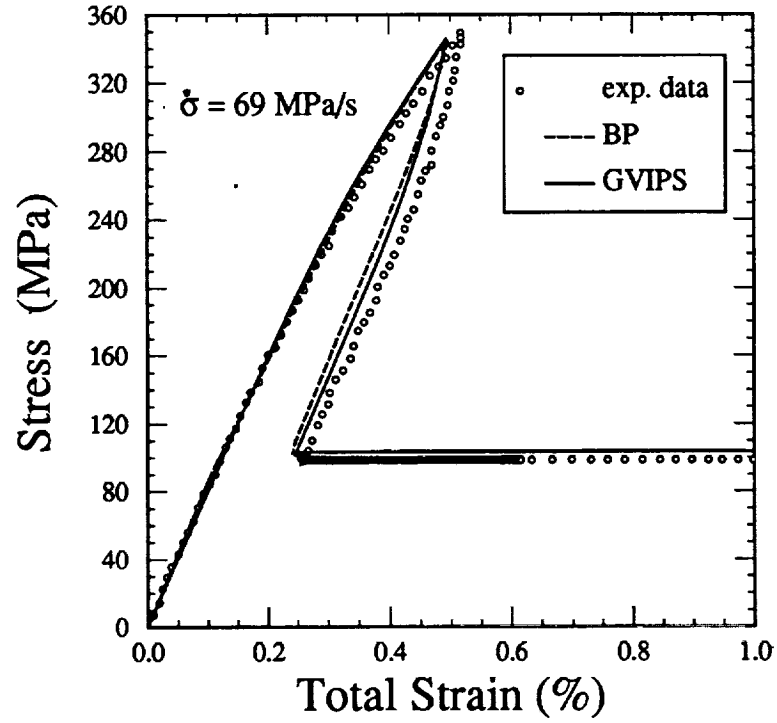

Figure 9: Plasticity - Creep interation test: stress-strain reponse simulation versus experimental data.

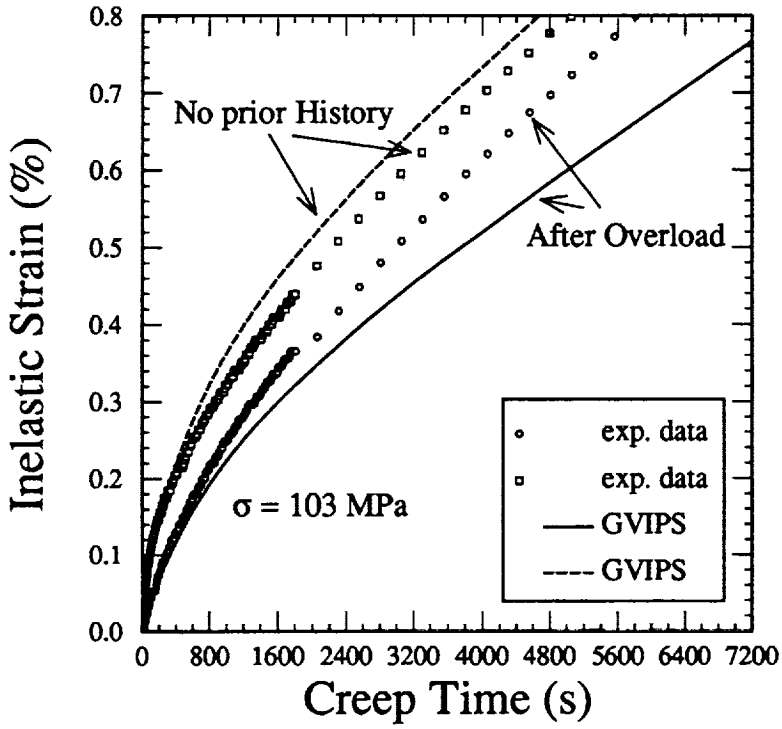

Figure 10: Plasticity - creep interation test: illustrating the influence of prior history on inelastic response.

6 GVIPS vs. BP Model

Reviewing figures 3 through 10 it is evident that the present GVIPS model in conjunction with the material parameters of Table 1 does a very good overall job of simulating the short term and small strain behavior of TIMETAL 21S at 650°C. In an attempt to assess the relative quality of these correlations and predictions as well as the numerical efficiency of the present model, an alternative and commonly employed unified viscoplastic model was implemented into our in-house Inelastic Deformation Analysis Code (IDAC). The full multiaxial, nonisothermal formulation of the Bodner-Partom (BP) model, given in [5] was chosen as the alternative model because it too has been characterized for the titanium matrix TIMETAL 21S. The specific tests employed to characterize this model are unknown to the authors, thus all of the previous loading conditions will be investigated and assumed to be predictions.

Figures 11 through 15 illustrate the tensile, creep, cyclic, and relaxation behavior predictions of the BP model at 650°C. The corresponding GVIPS simulations are also included in these figures for ease of comparison. Examining Fig. 11 it is apparent that at the higher strain rates (8.33×10^{-5} and 8.33×10^{-4}) the BP model does a better job of predicting the saturated stress values at 0.01 strain than does the GVIPS model. However, at the lower strain rates the BP model does a poorer job in representing the knee (or transient portion) of the tensile curves. This poorer simulation by the BP model of the time dependent behavior is further illustrated in Figs. 12, 14, and 15, wherein the creep and relaxation behavior is compared with the GVIPS simulations. Clearly, both the primary and secondary creep rates differ greatly and disagree with the experimental observations. Similarly, the short and mid term BP relaxation response is inaccurately predicted in Figs. 14 and 15 as compared with the more accurate GVIPS simulations. This inferior performance in creep and relaxation is not unexpected as the BP model is known for its ability to predict the rate-dependent tensile and cyclic response of a material and not the time-dependent creep and relaxation behavior. The significance of this failure to adequately

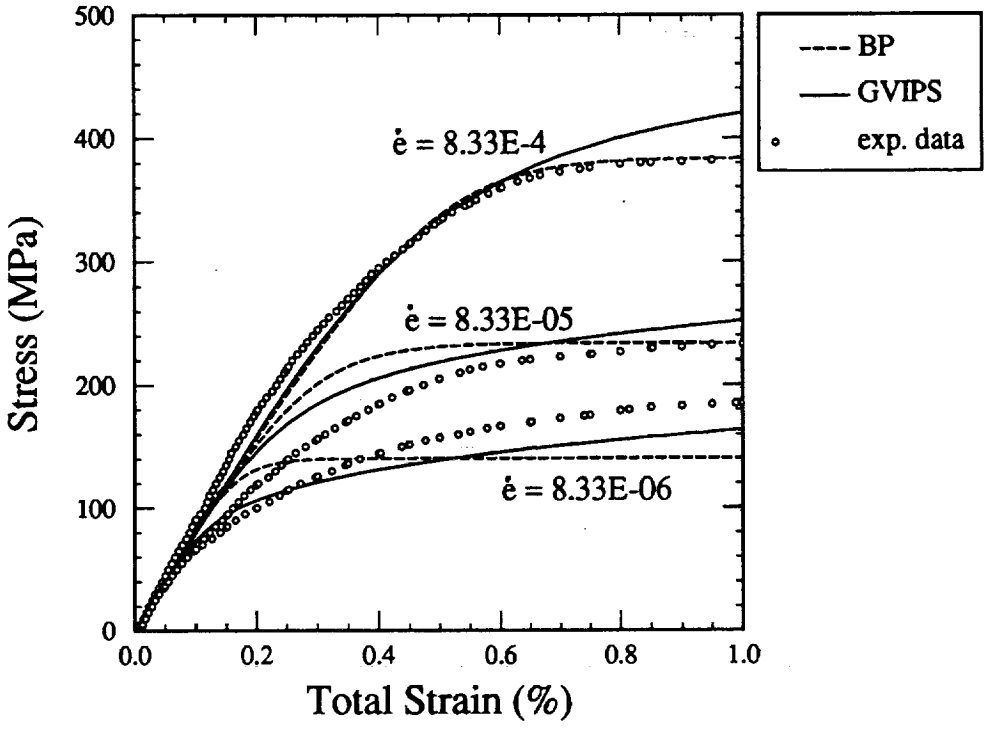

Figure 11: GVIPS and BP simulation of the influence of strain rate on the tensile response.

capture the time-dependent behavior is further emphasized in both the multi-step creep test shown in Fig. 8 and the plasticity-creep interaction test shown in Figs. 9 and 16 wherein the BP model poorly represents the primary creep (transient or short term response) following a change in the applied loading.

The ability of the BP model to simulate the rate-dependent cyclic behavior is shown in Figs. 7 and 13, where both the BP and GVIPS responses are in reasonably good agreement, except for the predicted maximum stress amplitudes achieved, where they differ between 10% and 30% of one another. Also, note that in Fig. 13 a numerical problem was observed in the BP model during unloading at the fastest strain rate of 8.33×10^{-4}. No special numerical techniques where implemented to attempt to overcome this difficulty as suggested in the work of Kroupa [5], because a strict comparison in the numerical integration of these two models was desired.

Finally, a comparison of the numerical efficiency of both models is made, relative to the total number of integration steps required to complete the above simulations. This comparison is completely legitimate as both multiaxial models were implemented into the same computer code, integrated using the same self-adapting fourth order Runge-Kutta and Adams Bashforth predictor-corrector integration algorithm, and executed on the same Sun IPX workstation. Table 2 contains the number of total integration steps required to perform each loading history discussed. Clearly, the GVIPS model is extremely easy to integrate (due to the use of power law material functions as opposed to exponential ones and the potential structure itself) when compared with the BP model and therefore would provide significant computational savings in a large-scale structural finite element analysis. Note that in the case of tensile and cyclic behavior both models give similar accuracy and yet the GVIPS formulation provides at least a factor of 2 improvement in numerical efficiency over the BP model. Furthermore, in the case of creep and relaxation where the simulation accuracy of GVIPS is clearly superior to the BP model, the numerical efficiency is also superior, particularly in the case of creep where numerical stiffness can become a problem [21]. Thus the GVIPS (generalized viscoplasticity with potential structure) formulation provides not only accurate predictive capability, but also superior numerical performance over other non-potential

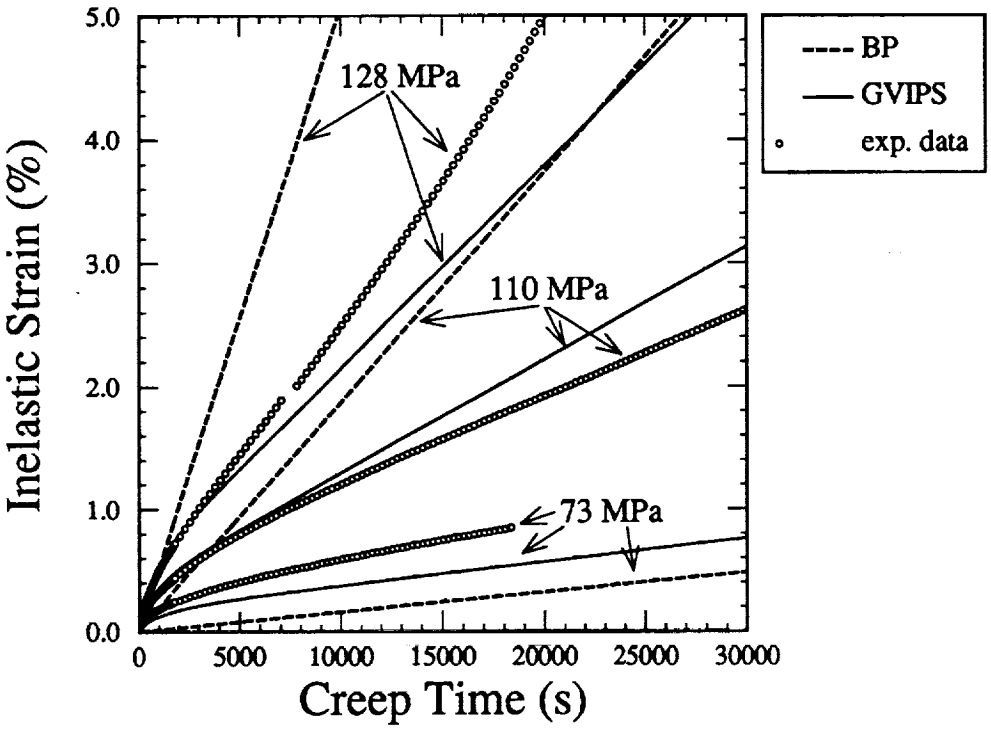

Figure 12: GVIPS and BP simulation of the creep response.

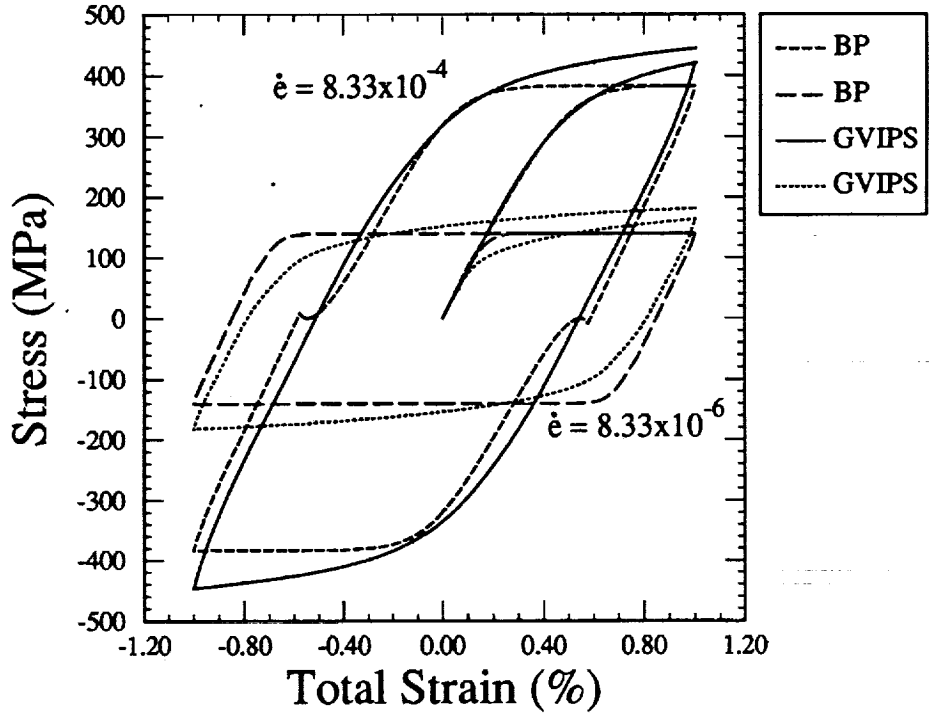

Figure 13: GVIPS and BP simulation of cyclic behavior with two orders of magnitude difference in total strain rate.

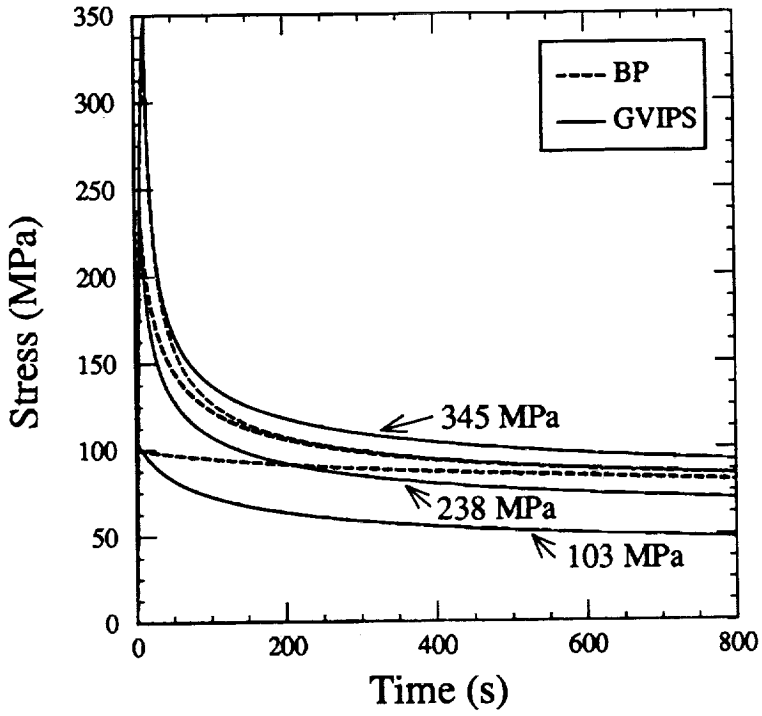

Figure 14: GVIPS and BP simulation of short term relaxation response.

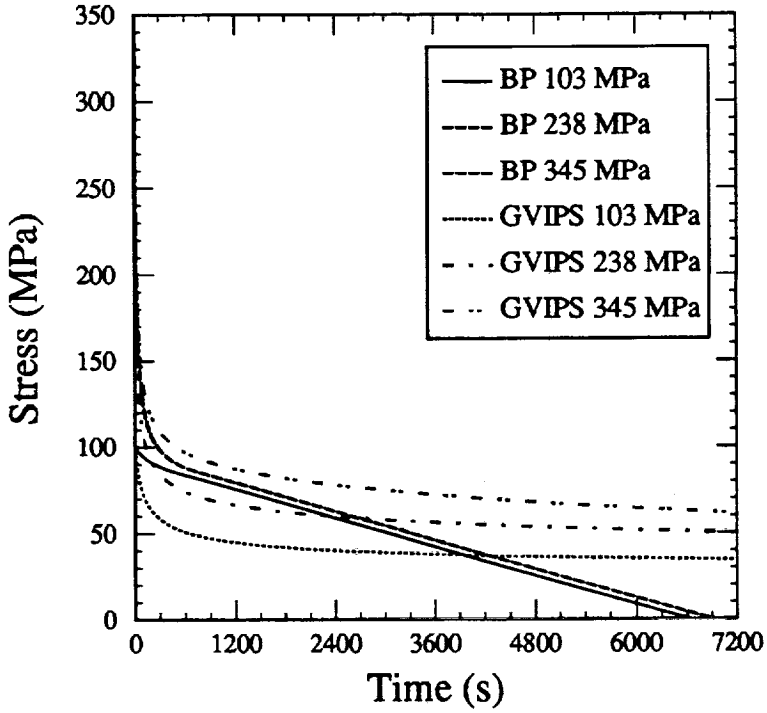

Figure 15: GVIPS and BP simulation of mid term relaxation response.

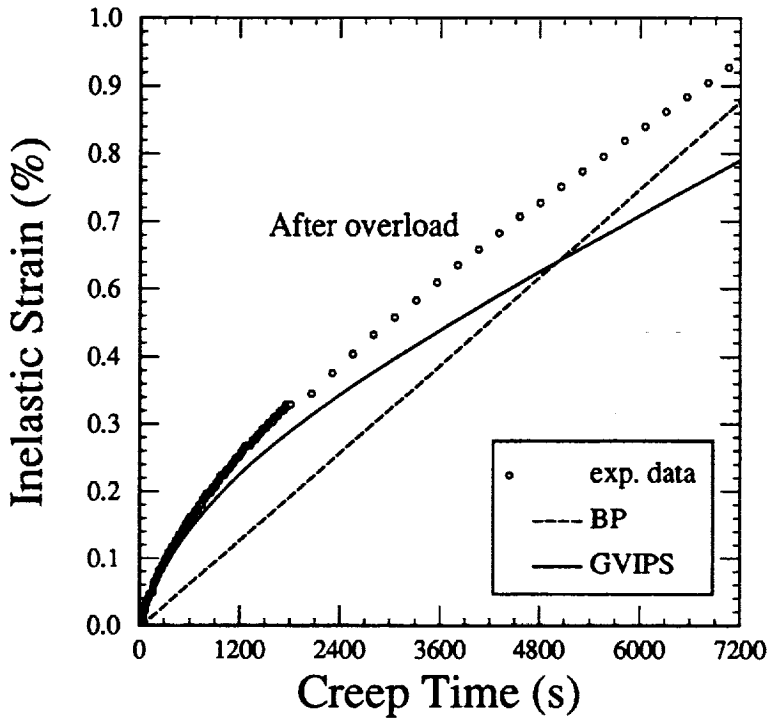

Figure 16: GVIPS and BP simulation of inelastic (creep) response following overload shown in Fig. 9.

Type of Test	Integration Steps		Speed-up
	GVIPS	BP	
Tensile (1/sec)			
$\dot{e} = 8.33\text{x}10^{-4}$	170	338	1.99
$= 8.33\text{x}10^{-5}$	196	619	3.16
$= 8.33\text{x}10^{-6}$	231	992	4.29
Cyclic (1/sec)			
$\dot{e} = 8.33\text{x}10^{-4}$	761	15007	19.72
$= 8.33\text{x}10^{-5}$	828	2727	3.29
$= 8.33\text{x}10^{-6}$	938	4937	5.26
Creep (MPa)			
$\sigma = 72.4$	335	758	2.26
$= 110$	359	12203	34
$= 128$	364	32621	89.6
Relaxation (MPa)			
$\sigma = 345$	372	624	1.68
$= 238$	365	519	1.42
$= 103$	358	382	1.07
4 Step Creep Test	1189	6631	5.57
Plasticity/Creep	476	8839	18.5

Table 2: Numerical Comparison of the GVIPS and BP Models

formulations, the BP model being an example.

7 Summary

A fully associative, multiaxial, isothermal, nonlinear kinematic hardening viscoplastic model has been presented. It contains in general, three internal state variables (two scalars and one tensor) and both thermal and strain-induced recovery mechanisms. The two, non-evolving, scalar internal state variables are associated with dislocation density and are defined as the drag and yield stress. The evolving tensorial variable known as the internal (or back) stress is a second order, traceless, symmetric tensor and is associated with dislocation substructure. A unique aspect of the present model is the inclusion of non-linear hardening through the use of a compliance operator, derived from the Gibb's potential, in the evolution law for the back stress. This non-linear tensorial operator is significant in that it allows both the flow and evolutionary laws to be fully associative (and therefore easily integrated) and greatly influences the multiaxial response under non-proportional loading paths. In addition to this nonlinear compliance operator, a new consistent, potential preserving, internal strain unloading criterion has been introduced to prevent abnormalities in the predicted stress-strain curves, which are present with nonlinear hardening formulations, during unloading and reversed loading of the external variables. The resulting isothermal unified viscoplastic model was then characterized for the titanium based alloy TIMETAL 21S at 650°C. Results illustrated the good overall correlation and predictive capabilities of the model for a wide range of loading conditions, that is tensile, cyclic, creep, and relaxation tests. The proposed model was then compared with a commonly accepted and employed version of the Bodner-Partom viscoplastic model and was found to be superior both in its predictive capabilities and numerical performance.

8 Acknowledgement

The authors would like to acknowledge the efforts of Dr. T.E. Wilt in the development of IDAC and implementation of both the GVIPS and Bodner-Partom models. We would also like to thank him for his assistance in performing a number of the simulations presented in this paper.

References

[1] Arnold, S.M.; and Saleeb, A.F.: On the Thermodynamic Framework of Generalized Coupled Thermoelastic Viscoplastic - Damage Modeling. NASA TM-105349, 1991.

[2] Saleeb, A.F. and Wilt, T.E.: Analysis of the Anisotropic Viscoplastic-Damage Response of Composite Laminates-Continuum Basis and Computational Algorithms, Int. Jnl. Num. Meth. Engng., Vol. 36, 1993, pp. 1629-1660.

[3] Arnold, S.M., Saleeb, A.F, and Wilt, T.E.: A Modeling Investigation of Thermal and Strain Induced Recovery and Nonlinear Hardening in Potential Based Viscoplasticity, NASA TM-106122, 1993.

[4] Saleeb,A.F., Seif, Y., and Arnold, S.M.: Fully-Associative Viscoplasticity with Anisotropic and Nonlinear Kinematic Hardening, submitted Int. Jnl. of Plasticity, 1994.

[5] Kroupa, J.L.: Implementation of a Nonisothermal Unified Inelastic-Strain Theory Into ADINA 6.0 for a Titanium Alloy - User Guide, WL-TR-93-4005, 1993.

[6] Bodner, S.R. and Partom, Y.:Constitutive Equations for Elastic-Viscoplastic Strain Hardening Materials, Jnl. Appl. Mech., Vol. 42, 1975, pp. 385.

[7] Chan, K.S.,Bodner, S.R., and Lindholm, U.S.: Phenomenological Modeling of Hardening and Thermal Recovery in Metals, Jnl. Engng. Mat. and Tech., Vol. 110, 1988, pp.1-8.

[8] Stouffer, D.C., Ramaswamy, V.G., Laflen, J.H., Van Stone, R.H., and Williams, R.: A Constitutive Model for the Inelastic Multiaxial Response of Rene'80 at 871C and 982C, Jnl. Engng. Mat. Tech., Vol. 112, 1990, pp. 241-246.

[9] Spencer, A.J.M.: Continuum Physics, Vol. 1, A.C. Eringen, Ed., Academic Press., London, 1971, p. 240.

[10] Arnold, S.M.: Effects of State Recovery On Creep Buckling Induced By Thermomechanical Loading. Ph.D. Thesis, University of Akron, Akron, OH, 1987.

[11] Onat, E.T.; and Fardshisheh, F.: Representation of Creep of Metals. ORNL TM-4783, 1972.

[12] Onat, E.T.; and Fardshisheh F.: Representation of Creep, Rate Sensitivity and Plasticity, SIAM J. Appl. Math., vol. 25, no. 3, 1973, pp. 522-538.

[13] Lemaitre, J.; and Chaboche, J.L.: Mechanics of Solid Materials, Cambridge University. Press, New York, 1990.

[14] Orowan, E.: Causes and Effects of Internal Stresses, Internal Stresses and Fatigue of Metals, Proceedings of the Symposium on Internal Stresses and Fatigue in Metals, Detroit Mich., Eds., G.M. Rassweiler and W.L. Grvise, Elsevier Publishing, 1959.

[15] Robinson, D.N.: A Unified Creep -Plasticity Model for Structural Metals at High Temperature. ORNL TM-5969, 1978.

[16] Robinson, D.N; and Swindeman, R.W.: Unified Creep-Plasticity Constitutive Equations for 2 1/4 Cr-1Mo Steel at Elevated Temperature, ORNL TM-8444, 1982.

[17] Miller, A.K., Ed.: Unified Constitutive Equations for Plastic Deformation and Creep of Engineering Alloys, Elsevier Applied Science, New York, 1987.

[18] Freed, A.D.; Chaboche, J.L.; and Walker, K.P.: A Viscoplastic Theory with Thermodynamic Considerations, Acta Mech, vol. 90, 1991, pp. 155-174.

[19] Castelli, M.G., Arnold, S.M., and Saleeb, A.F.:Specialized Deformation Tests for the Characterization of a Viscoplastic Model:Application to a Titanium Alloy, NASA TM-106268, 1994.

[20] Ashbaugh, N.E., and Khobaib, M.: Unpublished Data, University of Dayton Research Institute, Dayton, Ohio.

[21] Arnold, S.M.: Quantification of Numerical Stiffness for a Unified Viscoplastic Constitutive Model, Jnl Engng. Mat. Tech., Vol. 112, 1990, pp.271-276.

REPORT DOCUMENTATION PAGE

Form Approved
OMB No. 0704-0188

1. AGENCY USE ONLY (*Leave blank*)	2. REPORT DATE	3. REPORT TYPE AND DATES COVERED
	June 1994	Technical Memorandum

4. TITLE AND SUBTITLE

A Fully Associative, Non-Linear Kinematic, Unified Viscoplastic Model for Titanium Based Matrices

5. FUNDING NUMBERS

WU-763-22-2F

6. AUTHOR(S)

S. M. Arnold, A. F. Saleeb, and M. G. Castelli

7. PERFORMING ORGANIZATION NAME(S) AND ADDRESS(ES)

National Aeronautics and Space Administration
Lewis Research Center
Cleveland, Ohio 44135-3191

8. PERFORMING ORGANIZATION REPORT NUMBER

E-8890

9. SPONSORING/MONITORING AGENCY NAME(S) AND ADDRESS(ES)

National Aeronautics and Space Administration
Washington, D.C. 20546-0001

10. SPONSORING/MONITORING AGENCY REPORT NUMBER

NASA TM-106609

11. SUPPLEMENTARY NOTES

Prepared for the Symposium on Life Prediction Methodology for Titanium Matrix Composites sponsored by the American Society for Testing and Materials, Hilton Head, South Carolina, March 22-24, 1994. S. M. Arnold, NASA Lewis Research Center; A. F. Saleeb, University of Akron, Department of Civil Engineering, Akron, Ohio 44325 (work funded by NASA Grant NAG3-901); and M. G. Castelli, NYMA, Inc., Engineering Services Division, 2001 Aerospace Parkway, Brook Park, Ohio 44142 (work funded by NASA Contract NAS3-27186). Responsible person, S. M. Arnold, organization code 5220, (216) 433-3334.

12a. DISTRIBUTION/AVAILABILITY STATEMENT

Unclassified - Unlimited
Subject Category 39

12b. DISTRIBUTION CODE

13. ABSTRACT (*Maximum 200 words*)

Specific forms for both the Gibb's and complementary dissipation potentials are chosen such that a complete (i.e., fully associative) potential based multiaxial unified viscoplastic model is obtained. This model possess one tensorial internal state variable, that is associated with dislocation substructure, with an evolutionary law that has nonlinear kinematic hardening and both thermal and strain induced recovery mechanisms. A unique aspect of the present model is the inclusion of non-linear hardening through the use of a compliance operator, derived from the Gibb's potential, in the evolution law for the back stress. This non-linear tensorial operator is significant in that it allows both the flow and evolutionary laws to be fully associative (and therefore easily integrated) and greatly influences the multiaxial response under non-proportional loading paths. In addition to this nonlinear compliance operator, a new consistent, potential preserving, internal strain unloading criterion has been introduced to prevent abnormalities in the predicted stress-strain curves, which are present with nonlinear hardening formulations, during unloading and reversed loading of the external variables. Specification of an experimental program for the complete determination of the material functions and parameters for characterizing a metallic matrix, e.g., TIMETAL 21S, is given. The experiments utilized are tensile, creep, and step creep tests. Finally, a comparison of this model and a commonly used Bodner-Partom model is made on the basis of predictive accuracy and numerical efficiency.

14. SUBJECT TERMS

Viscoplasticity; Nonlinear hardening; Isothermal; Deformation; Multiaxial; Correlations; Predictions

15. NUMBER OF PAGES
26

16. PRICE CODE
A03

17. SECURITY CLASSIFICATION OF REPORT	18. SECURITY CLASSIFICATION OF THIS PAGE	19. SECURITY CLASSIFICATION OF ABSTRACT	20. LIMITATION OF ABSTRACT
Unclassified	Unclassified	Unclassified	